New insights into the effects of growth phase and enzymatic treatment on the cell-wall properties of Chlorella vulgaris microalgae

Jérôme F.L. Duval, Angelina Razafitianamaharavo, Isabelle Bihannic, Marc Offroy, Nicolas Lesniewska, Bénédicte Sohm, Hélène Le Cordier, Christian Mustin, Christophe Pagnout, Audrey Beaussart

New insights into the effects of growth phase and enzymatic treatment on the cell-wall properties of *Chlorella vulgaris* microalgae

Jérôme F. L. Duval[1]*, Angelina Razafitianamaharavo[1], Isabelle Bihannic[1], Marc Offroy[1], Nicolas Lesniewska[1], Bénédicte Sohm[2], Hélène Le Cordier[1], Christian Mustin[1], Christophe Pagnout[2], Audrey Beaussart[1]*

[1] Université de Lorraine, CNRS, LIEC, F-54000 Nancy, France.

[2] Université de Lorraine, CNRS, LIEC, F-57000 Metz, France.

* Corresponding author:
jerome.duval@univ-lorraine.fr
audrey.beaussart@univ-lorraine.fr

ORCID
J.F.L. Duval : 0000-0002-5458-3761
I. Bihannic : 0000-0001-9780-2509
A. Beaussart : 0000-0002-4602-3019
A. Razafitianamaharavo : 0000-0002-7199-3017

KEYWORDS: chlorella, growth phase, atomic force microscopy, confocal, lysozyme, fibrils

GRAPHICAL ABSTRACT

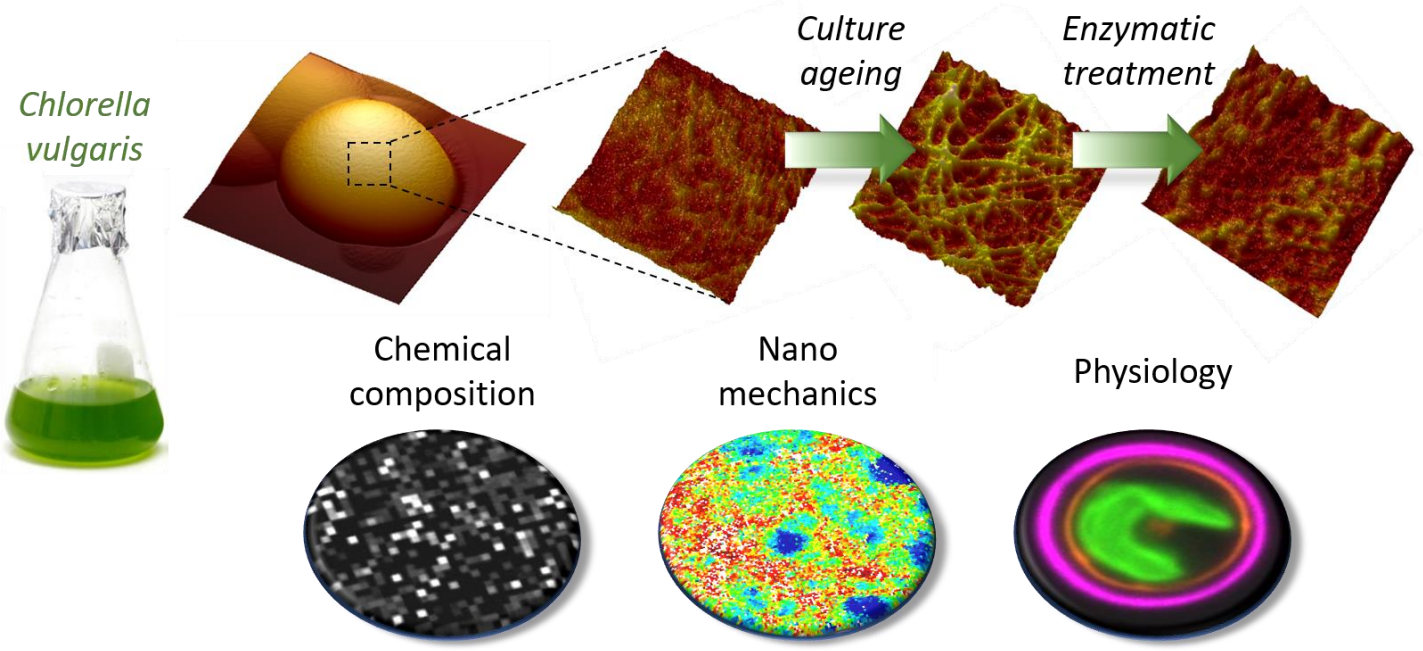

ABSTRACT

Green microalgae are a natural source of oil for commercial biodiesel production. However, their cell-wall barrier remains a major obstacle for effective intracellular lipid extraction. Solution to this issue includes the use of surface-digesting enzymes and the control of the so-far poorly understood changes in structural and mechanical properties of the microalgal envelops during growth and upon action of enzymes. Here, we used a combination of atomic force microscopy (AFM) and confocal microscopy to decipher the variation of cell-wall ultrastructure, composition and nanomechanics of *Chlorella vulgaris* upon culture ageing and lysozyme treatment. AFM imaging revealed the presence of a fibrillated mesh at the surface of cells harvested in the stationary phase, hardly distinguishable on cells from younger culture (mid-log phase). The fibrils form a chitin-like network containing the *N*-acetyl-D-glucosamine unit, and this structured network is severely damaged upon lysozyme treatment, a property we identified at the cellular and molecular scales by fluorescent-lectin staining and AFM-based force spectroscopy using lectin-modified tips, respectively. The enzyme was also found to act on algal physiology, to trigger oxidative stress and changes in cell lipid content. Detailed single-cell mapping of the nanomechanical properties of *C. vulgaris* further indicated that microalgal cells soften upon ageing and it confirmed that lysozyme affects both their surface and intracellular compartments. Altogether, our results emphasize that AFM-based multi-parametric analysis in combination with confocal microscopy allows accurate evaluation of physico-chemical surface properties of microalgae and offer an exciting perspective on cell culture condition optimization for facilitated oil extraction.

1. INTRODUCTION

Lipid-producing microalgae have raised great interest in the industrial sector as potential feedstock to generate biodiesel. They present the advantage to have a high oil yield and to grow easily on non-arable land with water that is unsuitable for human consumption. However, the development of proper technologies able to generate biofuel from microalgae at large scale is still in its childhood, mostly due to the high operating costs associated with cell harvesting, cell disruption and lipid extraction methods. The main limitation arises from the intrinsic rigidity of the microalgae cell-wall, forming a barrier between the intracellular space and its surrounding environment, which limits the access to the internal lipidic content. Several disruption technologies have already been suggested like solvent-mediated extraction,[1] bead milling,[2] high pressure homogenization[3] or ultrasonication.[4] Although efficient, these processes require large chemical or energy loads. As an alternative, Gerken *et al*. considered enzymatic digestion to permeabilise microalgae and they proposed the use of lysozyme as a pre-treatment to remove the protective layer at the surface of mature cells, thus allowing the access of other enzymes (*e.g.* chitinase) to substrates buried underneath.[5] More recent studies have also reported enzymatic treatments as an emerging substitute to mechanical degradation.[6]

Chlorella vulgaris is an important member of the eukaryotic green microalgae. This non-motile spherical auto-spore multiplies asexually and rapidly in freshwater environments, making *C. vulgaris* an excellent candidate for industrial lipid extraction. Due to its short replication time, ease to be cultivated and its well-documented sensitivity towards environmental pollution, *C. vulgaris* also serves as a convenient model to address fundamental questions related to the toxicity of various contaminants including heavy metals and pharmaceutical residues,[7, 8] it is further commonly employed in standardized ecotoxicological bioassays (*e.g.* standard ISO 8692:2012

Water quality – Fresh water algal growth inhibition test with unicellular green algae) and it is viewed as a good candidate for water bioremediation.[8-10] Regardless of whether the focus is on cell harvesting optimization, lipid extraction or addressing the ecotoxicological effects of contaminants, it is required that the physico-chemical properties of *C. vulgaris* cell walls are deciphered at the proper cellular and molecular scales to address the connection between structure and reactivity of cell surface.

In that respect, complexity stems from the dynamic nature of the algal cell surface whose characteristics fluctuate with time. Specifically, culture growth phase has been reported to play an important role on cell surface charge, hydrophobicity and density of functional groups.[11, 12] As a result, it is no surprise that cell aging impacts on pollutant biosorption[7] and affects the efficiency of biomass harvesting, may it be by flotation,[13] flocculation[14] or filtration.[15] Although cell wall structure and mechanical properties inherently affect the extent of cell disruption and the further extraction of their intracellular content such as lipids, to the best of our knowledge little is known on the changes in *C. vulgaris* cell wall properties upon culture aging.

Accordingly, in the current study we address the ultrastructure, chemical composition and mechanical properties (elastic modulus and cell turgor pressure) of *C. vulgaris* cell wall depending on growth phase by using different modalities (*i.e.* imaging, single-molecule force spectroscopy and indentation) of atomic force microscopy (AFM) combined to confocal microscopy. We analyse the changes of cell envelop structure, intracellular lipid production and the presence of reactive oxygen species (ROS) as the cells are cultivated for longer time, and we follow the evolution of these parameters upon enzymatic lysozyme treatment. Quantitative analysis of the cells nanomechanical response highlights the intertwined relationship between the intracellular and cell-wall properties of *C. vulgaris*, and it further illustrates the importance of combining

single-molecule and single-cell methodologies to address questions as complex as the multi-faceted action of enzymes on microalgae.

2. MATERIALS AND METHODS

2.1. Strain and culture conditions.

Cryo-stocks of *C. vulgaris* SAG 211-11b were unfrozen and cultured in BG11 medium (Gibco), under constant illumination (42 µmol/m^2/s), at 22 °C under 160 rpm agitation. After 7 days, 1 mL of preculture was introduced in 100 mL Erlenmeyer flask filled with 50 mL fresh BG11 medium and capped with sterile gauze for aeration, and incubated in the conditions described above. Microalgae were harvested at 6 or 20 days of cultures.

Growth curve were determined by sampling the same microalgae culture daily for 25 days and by measuring the OD_{686nm} using a UV-visible spectrometer Shimadzu, UV2501PC.

Lysozyme-treated cells were obtained by adding 25 µL of lysozyme (Sigma, stock solution at 20 mg/mL) per mL of the 20-days old algal culture (*i.e.* final concentration of 500 µg/mL), and cells were then cultivated for 12 hours in the conditions described above.

2.2. Atomic force microscopy measurements.

AFM measurements were performed at room temperature in PBS buffer (Sigma, 0.01 M Phosphate Buffer Saline 0.138 M NaCl, 0.0027 M KCl, pH 7.4) using a Fastscan dimension Icon with Nanoscope V controller (Bruker). Microalgae from the cell suspension prepared as detailed above were rinsed twice by centrifugation (6 min, 720 rcf) and resuspended in PBS buffer. Immediately after centrifugation, cells were deposited on a cleaned borosicate glass slide previously covered with a layer of polyethyleneimine (PEI, Sigma, Mw=750000g/mol). After 15 minutes, the glass

slide was gently rinsed with PBS to remove unattached cells and further AFM experiments were performed in PBS buffer without dewetting. AFM experiments were started immediately after introducing the sample in the AFM set up. However, given the time required for sample stabilisation and AFM data acquisition, especially for force mapping, maps have been recorded up to 3 hours after initial immersion in PBS. However, we did not observe any evolution in both the adhesion and mechanical properties of the samples upon immersion time.

Images were acquired in Peak Force Tapping mode using NPG silicon nitride tips (Bruker), with a peak force frequency of 1 kHz, a scan rate of 1 Hz and a setpoint of 5 nN. RMS (root mean square) values were determined using Nanoscope analysis software (Bruker; Rq values on 1.5 µm x 1.5 µm images after second order flattening).

Prior to each force spectroscopy measurement, a calibration was performed on a rigid substratum in order to determine the deflection sensitivity (nm/V) of the AFM tip. In turn, this leads to the accurate evaluation of the cantilever spring constant following thermal noise method.[16] Deflection sensitivity was systematically measured for each tip used for the experiments upon recording few force curves on glass surfaces, thus ensuring consistency between deflection sensitivity values we obtained. In case of aberrant outcome, the tip was displaced to another spot of the glass surface and sensitivity measurement was repeated.

For single-molecule experiments, AFM tips were functionalized with Concanavalin A (ConA; Sigma) or Wheat Germ Agglutinin (WGA; Sigma) lectins by covalent grafting using N-hydroxysuccinimide (NHS)/ 1-ethyl-3-(3-dimethylaminopropyl)-carbodiimide (EDC) chemistry. For that purpose, gold-coated AFM tips (NPG, Bruker) were cleaned in UV-ozone incubator for 10 minutes, rinsed with ethanol, and immersed overnight in a 1 mM 16-mercaptohexadecanoic acid thiols (10%; Sigma) – 1 mM 11-mercapto-1-undecanol thiol (90%; Sigma) diluted in ethanol,

rinsed with ethanol and dry with nitrogen. They were then immersed in 4 mL of ultrapure water containing 40 mg of NHS (Sigma) and 100 mg of EDC (Sigma). After 30 min, tips were rinsed in ultrapure water and immersed in the lectin suspension at 0.2 mg/mL for 1 hour, rinsed and stored in PBS until use.

All single-molecule experiments were performed in PBS supplemented with $MgCl_2$ (1 mM) and $CaCl_2$ (1 mM). Adhesion maps (Fig. 3) were obtained by recording 32 x 32 force -distance curves on 1.5 µm x 1.5 µm area at the algal surface, with a maximum applied force of 500 pN and a constant approach and retraction tip speed of 1 µm s^{-1}. Adhesion maps were reconstructed by calculating the adhesion force of the last peak of each force curve and displaying the value as a grey pixel (Fig. 3).

For nanomechanical analysis, measurements were recorded in peak force tapping mode using NPG probes (Bruker). 256 x 256 approach and retract curves were recorded on a 1.5 µm x 1.5 µm area at the algal surface at 1 Hz scan rate, *via* application of a 5 nN loading force.

2.3. Confocal imaging.

Confocal images have been recorded on a ZEISS Axio observer 7, equipped with a scanning head LSM 880. Microalgae from the cell suspension prepared as detailed above were rinsed twice by centrifugation (6 min, 2000 rpm), resuspended in PBS buffer. Lectin-staining was done in PBS supplemented with $MgCl_2$ (1 mM) and $CaCl_2$ (1 mM). To that end, 10 µL of FITC-conjugated WGA (Sigma) or FITC-conjugated WGA (Sigma) suspension at 1 mg/mL was added to 90 µL of cell suspension. Lipid membranes were stained by the FM4-64 (Invitrogen, stock solution at 500 µg/mL prepared in Ultrapure water) and added to the microalgae suspension to a final concentration of 5 µg/mL. ROS staining was done by adding 4 µL of H_2DCFDA (Invitrogen; stock solution prepared at 200 µM in DMSO) in 396 µL of algal suspension. Nile Red staining was done

by adding 20 µL of Nile Red (Sigma; stock solution prepared at 0.2 mg/mL in DMSO) in 380 µL of algal suspension. Staining was performed 15 minutes prior to imaging. After staining, 5 µL of the cell suspension was deposited between a glass cover and a glass coverslip and sealed using nail polish to avoid drying, and images were recorded using a 63x Plan Apochromat 60x/1.4 Oil objective. Transmission, autofluorescence (AF) and FM4-64 images were obtained under 561-nm diode laser illumination. FITC-lectins, Nile Red and H_2DCFDA images have been recorded under 488-nm and 514-nm argon-laser illumination. The detection ranges were as follow: 677-686 nm for AF; 508-552 nm for FITC-lectins; 641-659 nm for FM4-64; 534-623 nm for Nile Red and 525-579 nm for H_2DCFDA.

3. RESULTS AND DISCUSSION

3.1. AFM imaging of the algal surface

We first addressed how cell culture conditions impacted on the morphological features of microalgal surface by comparing AFM images of *C. vulgaris* harvested in the mid-log phase (6 days of growth; Fig. 1a; hereafter denoted as cells from young culture) or in the stationary phase (20 days of growth; Fig. 1a; hereafter referred to as cells from mature culture). Images were collected under liquid conditions at low applied forces (Fig. 1b).

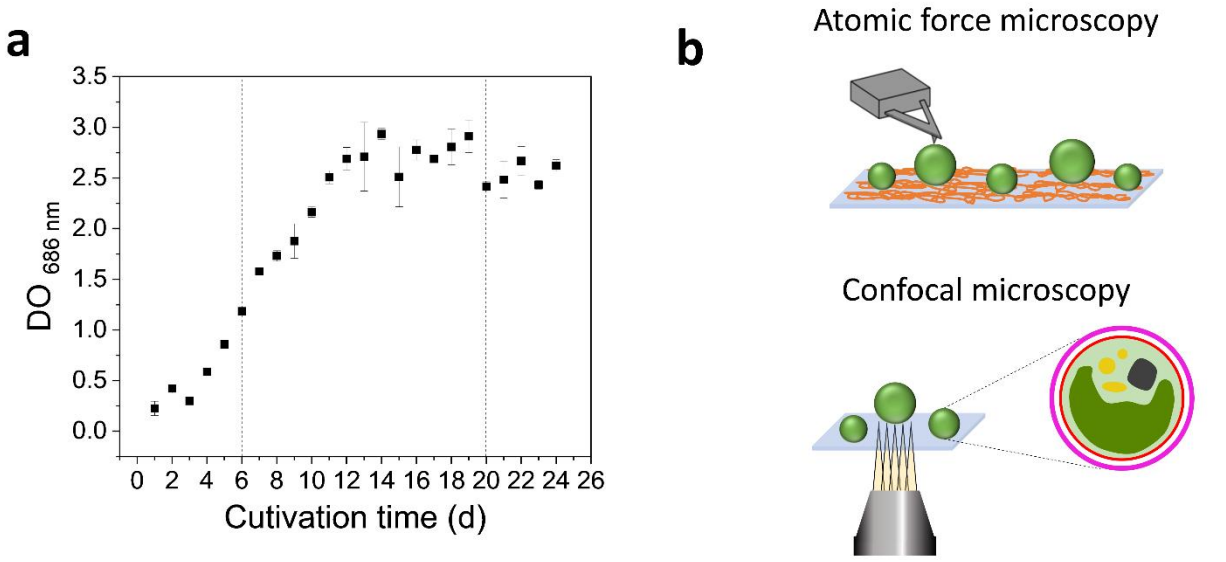

Figure 1. **Physico-chemical properties of cell-wall of *C. vulgaris* harvested at different growth phases are determined by a combination of AFM and confocal microscopy**. (a) Growth curve of *C. vulgaris* cultivated in BG11 media at 22°C under constant agitation. In the current study, algal properties are evaluated on cells harvested in the mid-log (6 days) and stationary (20 days) growth phases. Growth curves were obtained from 2 measurements on independent cultures. (b) Schematics of the AFM and confocal microscopy set-ups used.

Figs. 2a-b display representative peak force error images of *C. vulgaris* after 6 and 20 days of growth in BG11 at 22°C under constant agitation, respectively. Cells from the young culture exhibit a smooth surface (RMS = 3.0 ± 1.8 nm, median ± std calculated on n=17 cells) without any clearly distinguishable features except for the presence of few, thin filaments detected on some cell surface zones (Fig. 2a). Unlike their younger analogues, algae from the mature culture were significantly rougher (RMS = 8.2 ± 5.2 nm; n=16 cells) and displayed a mesh of fibrils of about 15 nm in height, entangled at their surface (Fig. 2b). These structures are reminiscent of the fibrillar structures observed by electron-microscopy at the surface of *Chlorella* strains, identified as chitin-like glycan by cell-wall hydrolysis and gas chromatography.[17, 18] As chitin is a long-chain polysaccharide composed of *N*-acetyl-D-glucosamine, we subjected cells from the mature culture

to an overnight treatment by lysozyme, an enzyme known to hydrolyse the 1,4-beta-linkages between N-acetylmuramic acid and *N*-acetyl-D-glucosamine residues in bacterial peptidoglycan.[19, 20] Lysozyme has already been reported to increase *Chlorella* cell-wall permeability, thus facilitating intracellular extraction,[5] but its exact mode of action has not been deciphered yet. As illustrated by Fig. 2c, fibrillar structures imaged on the cells from mature culture are cleared from the cell surface after lysozyme-based treatment, thereby leaving place to a surface similar to that of the cells from young culture albeit defined by a somewhat larger roughness (Fig. 2a; RMS = 5.3 ± 2.2 nm; n = 8 cells).

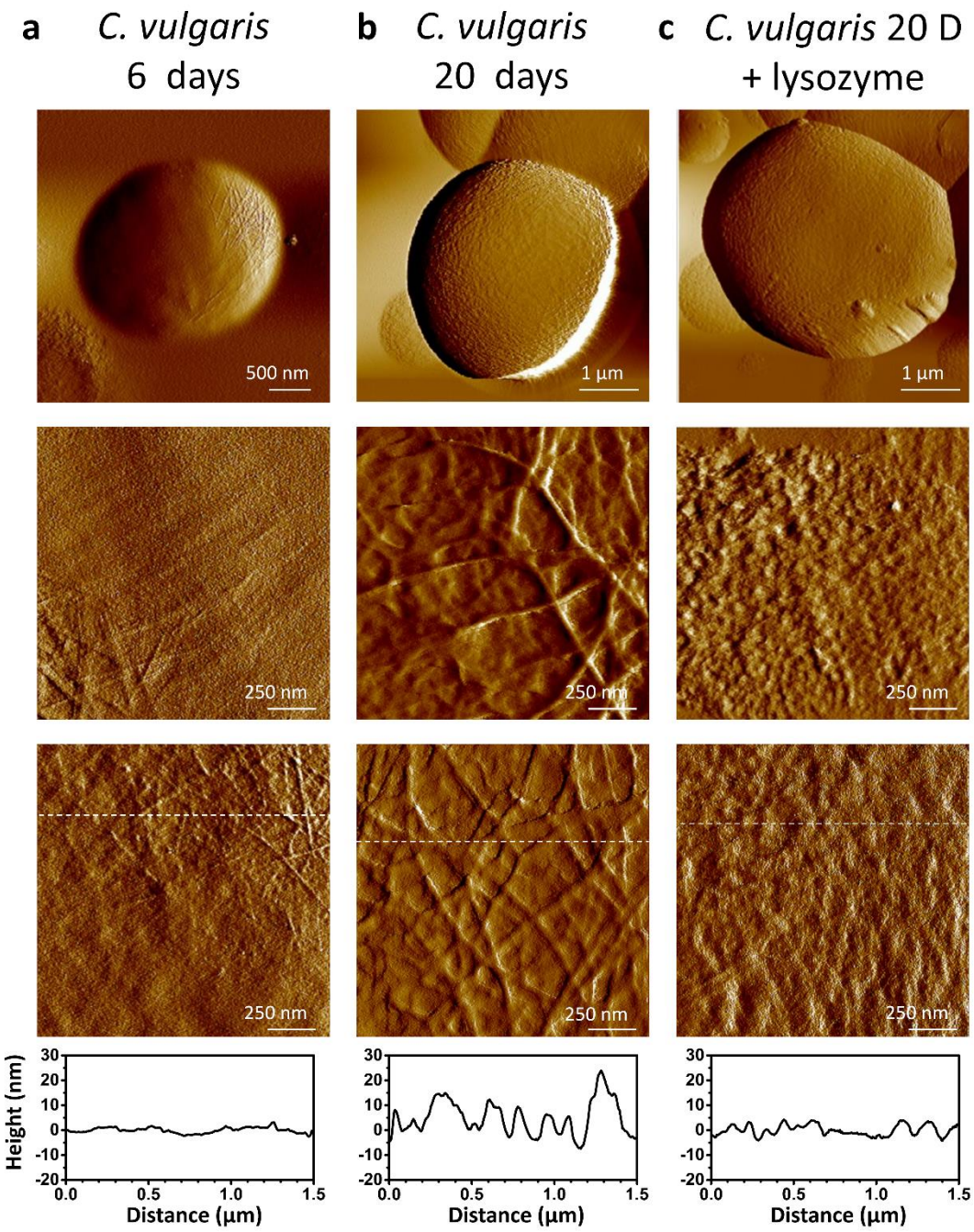

Figure 2. Representative AFM peak force error images of living *C. vulgaris* cells. (a-c) Low (top row) and high (middle and bottom rows) magnification images of cells from young (a), mature (b) and lysozyme-treated mature (c) cultures. The profiles underneath the images correspond to the vertical cross-sections taken along the dashed lines displayed in the corresponding height images, highlighting the larger roughness of the surface of cells from mature culture as compared to that of cells from young and lysozyme-treated cultures.

3.2. Identification of the fibrils composition by single-molecule force spectroscopy

We then used AFM tips decorated with the lectin wheat germ agglutinin (WGA) to confirm the chemical nature of the fibrils imaged in Fig. 2b at the surface of cells from mature culture and to map the spatial distribution of the *N*-acetyl-D-glucosamine residues that supposedly constitute these fibrils. Fig. 3a reports illustrative force adhesion maps featuring the presence and magnitude of tip-to-algal surface adhesion events as well as the corresponding adhesion force histograms collected on cells from the 20-days old culture. Results evidence a significant fraction (41%, n=3072 force curves from three independent experiments) of adhesive events randomly distributed all over the cell surface. We suggest that these adhesive events are specific of the WGA/*N*-acetyl-D-glucosamine bonds and there are several reasons that motivate such a correspondence. First, the distribution of the frequency of adhesion forces displays a maximum at around 60 pN, typical of the force values reported for lectin/sugar interactions.[21-23] Forces up to 400 pN were also detected albeit with lower frequency, and they reflect the detection of multiple lectin-carbohydrate bonds. Secondly, force *versus* separation distance curves corresponding to single-adhesive event could be fitted to the Worm-Like-Chain (WLC) model that is classically adopted for protein unfolding (red curve on Fig 3a),[24] due here to the unfolding of the lectin attached to the tip through a PEG-linker when withdrawing tip from the cell surface. Third, the frequency of adhesion events was significantly reduced under the following conditions: WGA-decorated tips interacting with lysozyme-treated cells (8% adhesion, Fig. 3b); tips decorated with Concanavalin A (ConA)- a lectin with high affinity for mannose and glucose[25]- interacting with cells from mature culture (12% adhesion, Fig. 3c); bare tips interacting with cells from mature culture (8% adhesion, Fig. 3d); and WGA-decorated tips interacting with cells from young culture (3% adhesion, Fig 3e).

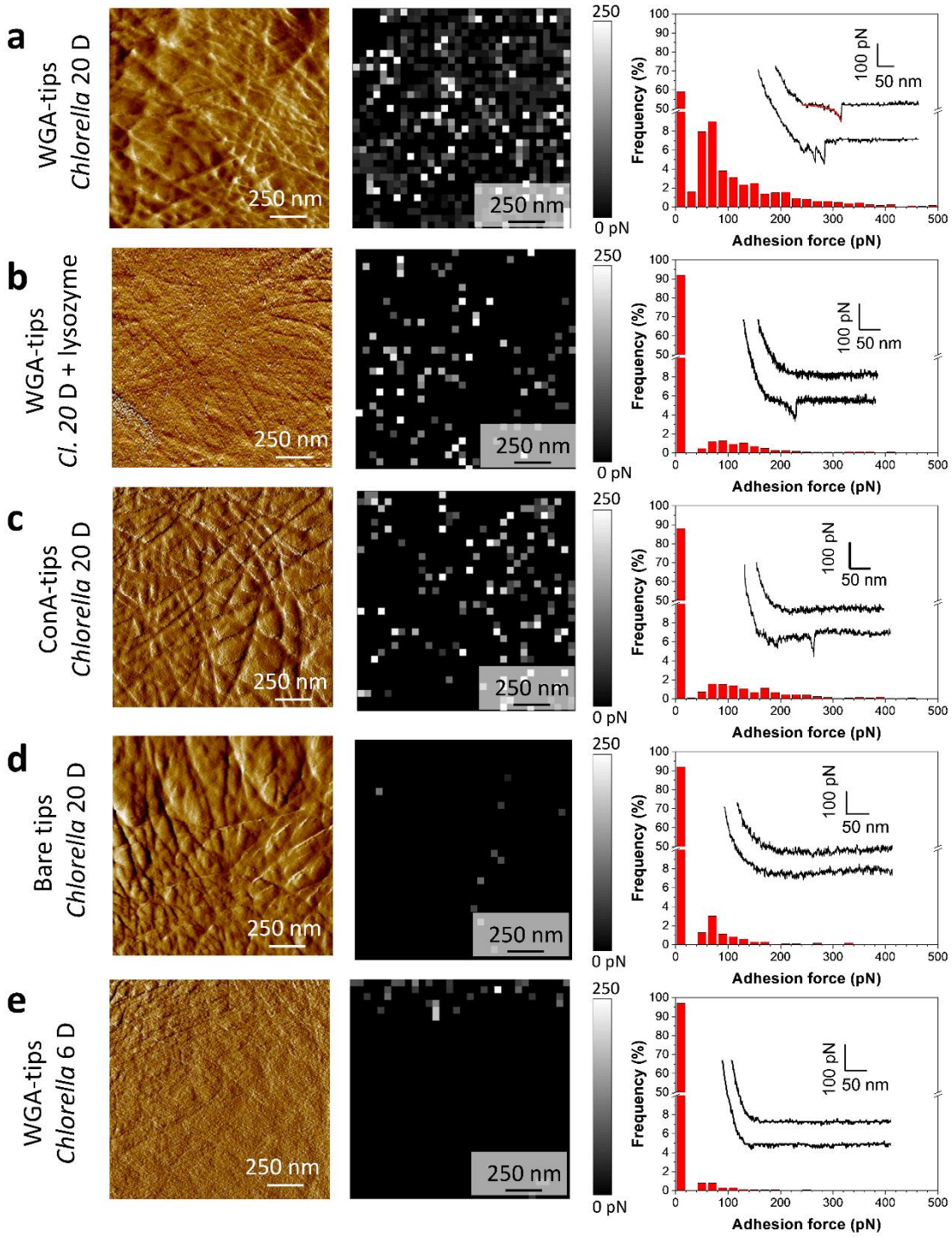

Figure 3. Molecular mapping of the *N*-acetyl-D-glucosamine unit at the algal surface. Peak force error images (left column), adhesion force maps (middle column) and corresponding adhesion histograms (right column) together with representative force curves recorded between AFM tips either bare (d) or decorated with WGA (a, b, e) or ConA (c) lectins and the surface of cells from young (e), mature (a, c, d) and lysozyme-treated mature (b) cultures. Each histogram of WGA-tip (a, b and e) was constructed from 3072 force-distances curves obtained on 3 cells from independent culture and using 3 different functionalized tips. Each histogram of controls experiments (ConA-tip in c and bare tip in d) was plotted from 2048 force-distances curves.

3.3. Confocal imaging of the chitin-like layer

To further confirm the presence of a peripheral *N*-acetyl-D-glucosamine layer on cells from mature culture, we performed confocal microscopy imaging on microalgae harvested in the stationary phase and stained with WGA-FITC dye (Fig. 4a). The cells stained with WGA-FITC showed an intense fluorescence at the cell periphery under 488-laser irradiation (Fig. 4a), thus confirming that the cell-wall of mature *C. vulgaris* contains amino sugars with structure similar to that of chitin and chitosan and composed of *N*-acetyl-D-glucosamine repeating units, as already reported for the *Chlorella* genus.[7, 26-28] For the sake of clarity in Fig. 4, WGA-FITC stained cell wall structures have been false-coloured in pink and the algal autofluorescence (AF) marked in green, although FITC maximum emission is around 520 nm and AF is above 650 nm. After treatment with lysozyme, the WGA-FITC-stained circle in Fig 4 representative of the chitin-like layer at the microalgae surface became incomplete for some of the cells we imaged and some tatters of stained structures could be further observed in solution (Fig. 4b). The shape of these cellular fragments reminds of the structures typically obtained after hydrolysis-based extraction of chlorella cell-wall.[17] These results evidence that the *N*-acetyl-D-glucosamine network partially detaches from the algal surface upon action of lysozyme, and we may not exclude the removal of other cell-wall components as well. It is emphasised here that the moderate lysozyme concentration adopted in our study was intentionally adopted so as not to fully remove the algal-cell wall and obtain protoplasts,[29] as the latest would then be too fragile to further perform the AFM indentation experiments we detail below.

Staining cells from the mature culture with ConA-FITC did not result in a detectable signal by confocal microscopy (Fig. 4c), which agrees with the single-molecule AFM results displayed in

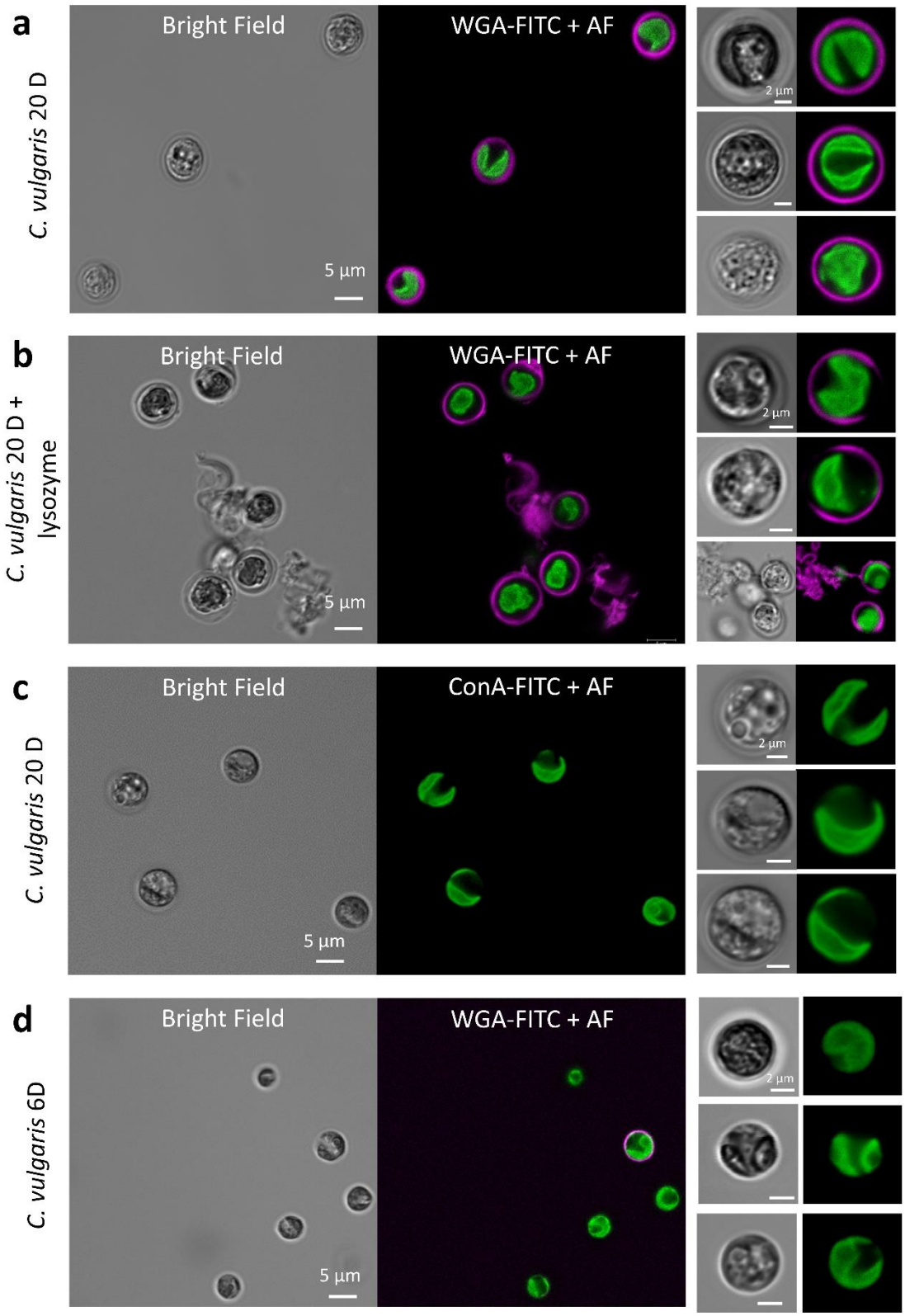

Figure 4. Confocal images reveal the presence of a chitin-like layer at the surface of mature cells. Bright field and confocal images of cell autofluorescence (denoted as AF) and WGA-FITC (a, b, d) or ConA-FITC (c) stained structures on cells from mature (a, c), lysozyme-treated mature (b) and young (d) cultures. WGA-FITC stained structures and AF have been false-coloured in pink and green, respectively.

Fig. 3c for tips decorated by the same ConA lectin (only 12% of the total amount of recorded force curves correspond to decorated tip-to-cell surface adhesion events). Finally, in support of AFM measurements (Fig. 3e), young culture did not display any fluorescence signal after their staining with WGA-FITC, except for a few cells, larger in diameter, which might be at different development stage leading to a certain heterogeneity within cell population. This associated heterogeneity in cell physiology is even exacerbated in the stationary phase.

3.4. Effects of lysozyme treatment on cell physiology

Lysozyme has been largely employed in industrial applications (*e.g.* as antimicrobial agent) mainly for its ability to enzymatically hydrolyse recalcitrant microbial cell-walls.[19, 20] However, the mode of lysozyme action extends well beyond its primary enzymatic function because it may *e.g.* inhibit the synthesis of DNA/RNA or even induce autolysin production.[30-32] Of particular interest for the biofuel production sector is the fact that enzymatic treatments -especially those including lysozyme- enhance lipid extraction yield at the scale of the algal suspension.[33, 34] However, the mechanisms operative at the cellular scale that underly such an enhanced macroscale productivity of biomass still remain unclear. Previous studies have reported an enlargement of the intracellular lipid droplets and accumulation of starch in microalgae subjected to an external stress such as nitrogen starvation.[35-37] Based on this finding, we hypothesize that enhanced lipid extraction yield following lysozyme treatment arises from combination of cell-wall weakening and increased production of lipids *via* an expansion of the lipid droplets following oxidative stress induced by lysozyme action. To validate this hypothesis, we performed confocal microscopy imaging after staining microalgae with dihydrofluorescein diacetate dye (H_2DCFDA; Figs. 5a-c) that marks Reactive Oxygen Species (ROS) and with Nile red dye that marks intracellular lipid droplets (Figs. 5d-f). Measurements were carried out on cells from young culture (Figs. 5a,d), cells from mature

culture (Figs. 5b,e), and cells from mature culture treated by lysozyme (Fig. 5c,f). Although ageing did not lead to significant oxidative stress (Fig. 5b), lysozyme treatment substantially enhanced ROS production, mostly located at the periphery of the algal cells (Fig. 5c).

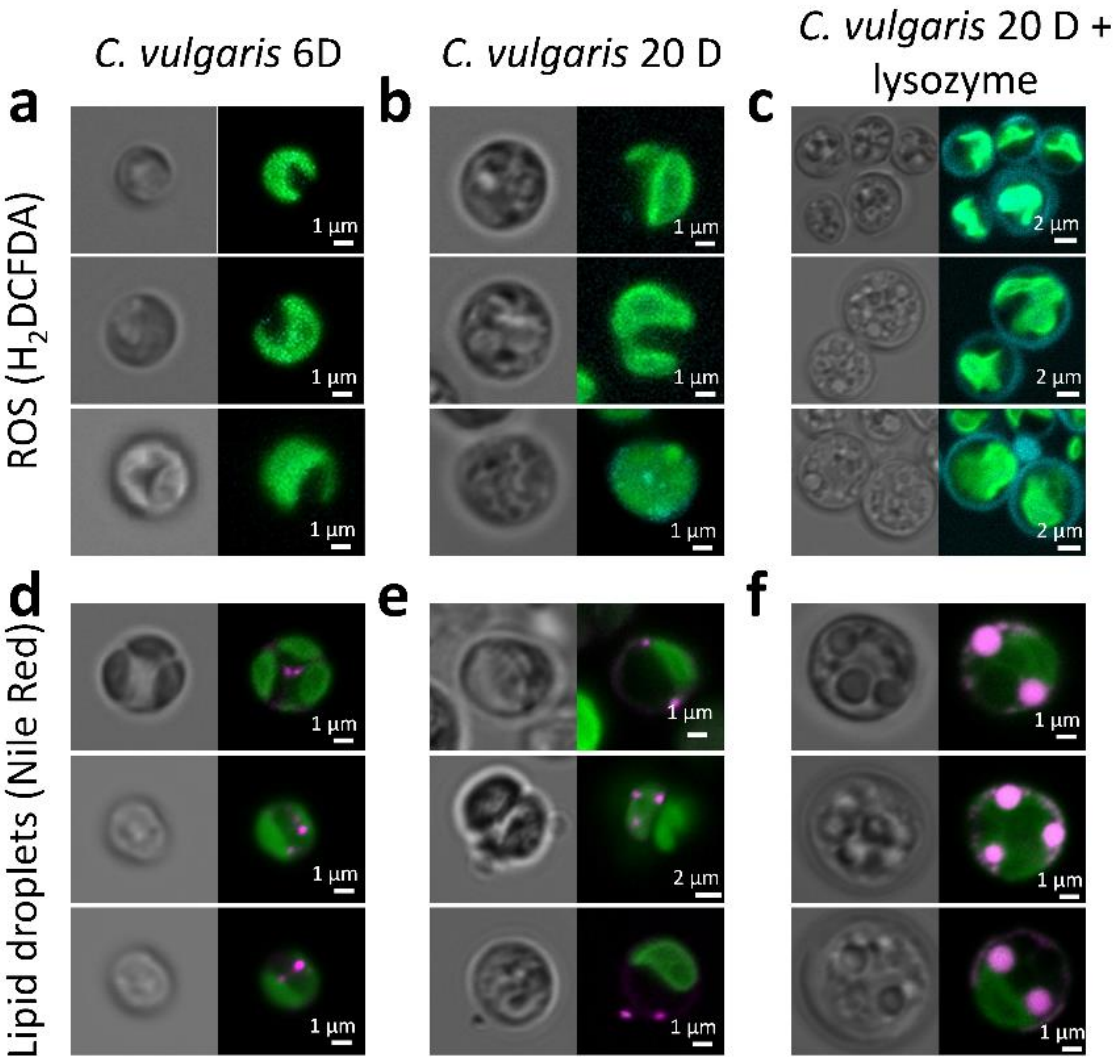

Figure 5. Effects of the lysozyme treatment on cell physiology. Bright field and confocal images of the autofluorescence (AF) and Nile red (bottom row) or H_2DCFDA (top row) stained structures obtained on algae from young (a), mature (b) and lysozyme-treated mature (c) cultures. Nile Red, H_2DCFDA stained structures and AF have been false-coloured in pink, cyan and green, respectively.

Accordingly, no significant changes in size of the detected lipid droplets could be observed between cells from young culture (397 ± 101 nm in diameter measured on 6 droplets, Fig. 5d) and cells from mature culture (436 ± 125 nm, measured on 7 droplets, Fig. 5e), and the average lipid droplet diameter significantly increased upon lysozyme treatment (1323 ± 196 nm measured on 8 droplets; Fig. 5f). These results strongly support the idea of a dual effect of lysozyme-based treatment and ensuing increase in microalgal lipid extraction, namely: a destabilization of the rigid cell-wall structure and an increased yield of intracellular lipids.

3.5. Nanomechanical properties of the algal cell-wall probed by AFM-based force spectroscopy.

To quantify the nanomechanics of the algae and the changes induced by cell ageing and lysozyme, we evaluated the spatial-distribution of cell-wall nanomechanical properties at various locations of the cell surface upon indentation of a Si_3N_4 AFM tip (Fig. 6). To that end, 256x256 force curves were recorded over 1.5 μm x 1.5 μm cell surface area. For each probed pixel of the cell surface, the measured force *versus* indentation curve is characteristic of that typically expected for turgescent cells[33-35] with two distinct indentation domains where the force varies with the indentation according to power and linear laws at sufficiently low and high values of the indentation (or equivalently force loads) (Fig. 6). Physically, the non-linear domain corresponds to the non-linear deformation of the cell envelop upon tip indentation and quantitative analysis according to the theory we detailed elsewhere[34] allows to retrieve the elastic (or Young) modulus of the probed surface structures of the cells, denoted hereafter as E (in Pa). The linear domain (also called the linear compliance regime) operational at higher applied forces results from the balance between internal cell turgor pressure and pressure exerted by the tip on the cell. The slope of that

domain is inherently determined by the spring constant of the tip (whose value is known, See Materials and Methods section) and the searched cell turgor pressure which is function of the cell stiffness denoted as k_{cell} (in N m^{-1}), also evaluated by modelling of the force *versus* indentation curves.[38-40] The indentation value marking the transition between the two aforementioned non-linear and linear domains of the measured force curve is further denoted as δ^* (in nm) (Fig. 6).

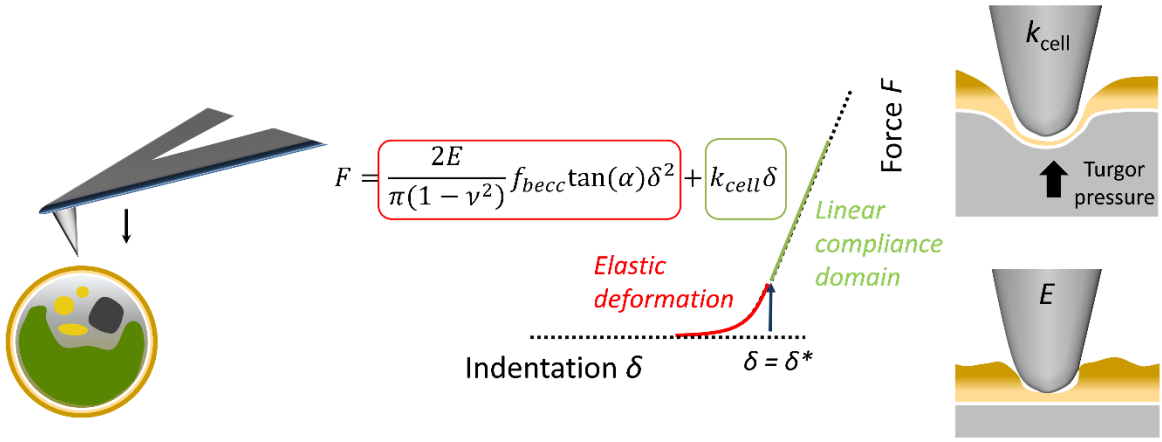

Figure 6. Schematic illustration of the method for evaluation of the nanomechanical properties of the algal surface by theoretical analysis of the nanoindentation force measurements. Force *versus* indentation curves comprise two successive domains upon indentation of the AFM tip into the cell envelop: a non-linear elastic deformation of the envelop, followed by a linear compliance domain. Analysis of the former regime leads to evaluation of the Young modulus (E) by the Sneddon model [41, 42] and that of the second regime to determination of the cell spring constant (k_{cell}, or cell stiffness) using the indicated equations. In this equation, ν is the Poisson ration (=1/2), f_{becc} is the bottom effect cone correction, and α is the AFM tip half opening angle of the cone (=17.5°). The reader is referred to [39] for details on the theoretical formalism.

As the AFM nanoindentation measurements are spatially resolved over the cell surface area (1 pixel corresponds to 1 measured force curve), the analysis makes it possible to generate maps of the retrieved Young modulus E, of values of the critical indentation δ^*, and of cell stiffness k_{cell} for cells from young (Fig. 7a), mature (Fig. 7b) and lysozyme-treated (Fig. 7c) cultures. Overall inspection of the three nanomechanical maps (E, δ^* and k_{cell}) associated with cell from mature

culture (Fig. 7b) display a heterogeneity that is more significant than that measured for cell from young culture (Fig. 7a) and lysozyme-treated cell (Fig. 7c), which is consistent with the setting of the fibrillated network (Fig. 2) embedded at the periphery of the only cells harvested in the stationary phase. Elasticity maps collected on smaller cell surface areas further highlight that the stiffest cell surface zones correspond to the fibrils (Fig. 7b, inset).

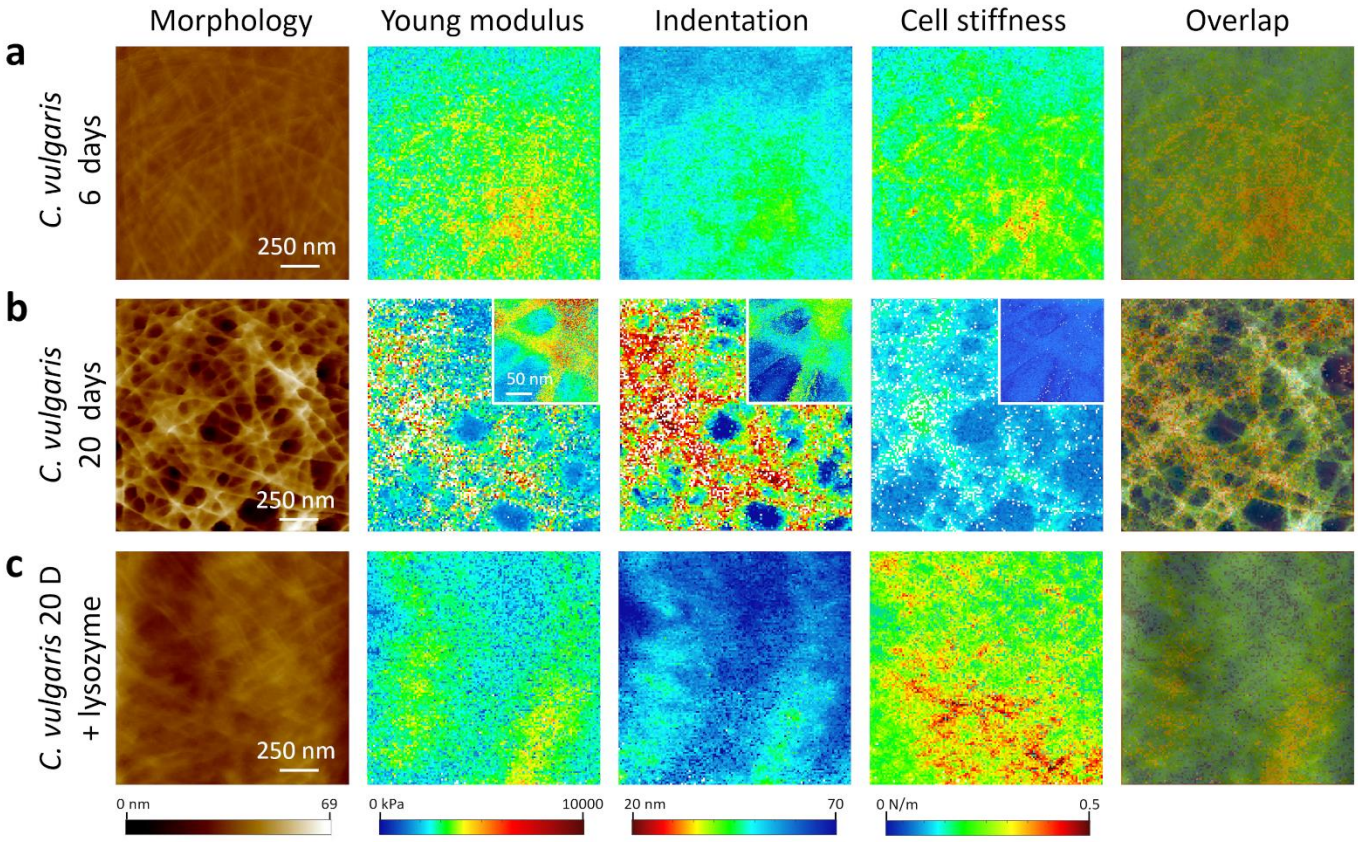

Figure 7. Nanomechanical properties of the microalgae depend on cell age. Representative Young modulus E, indentation $\delta^*$and cell stiffness k_{cell} maps of 256 x 256 pixels obtained by indenting 1.5 µm x 1.5 µm areas on cells from young (a), mature (b) and lysozyme-treated mature (c) cultures. Overlap of the peak force error (morphology) and Young modulus images illustrate that the stiffest regions (*i.e.* with the highest values of E) correspond to the zones of highest fibril density.

For the sake of further pragmatic analysis of the data reported in Fig. 7, all values of E, δ^* and k_{cell} determined over the 1.5 µm x 1.5 µm cell surface area for the 3 cell types were collated in the form of scatter plots featuring the dependence of δ^* on E (Fig. 8a-c, left panels) and that of k_{cell} on E (Fig. 8a-c, right panels). We clearly observe that the cloud of points in the δ^*- E representation is significantly spread for cells from the mature culture untreated with lysozyme (Fig. 8b) as compared to that pertaining to cells from young culture (Fig. 8a) and cells from lysozyme-treated culture (Fig. 8c). This feature reflects the differentiated spatial heterogeneities of the cell surface structure already invoked in Fig. 7 depending on the growth phase and enzyme treatment. For cells from the stationary phase culture (Fig. 8b), two δ^* *versus* E data clouds can be distinguished. Most likely, one is associated with the nanomechanical properties of the fibrils and the other corresponds to the underlying softer matrix and a thicker cell wall, as previously reported for *C. vulgaris* in the stationary phase. [43]

Interestingly, whereas the morphology of the cells from the young culture is rather similar to that of the lysozyme-treated cells (Figs. 2, 3 and 7), the mechanical properties of the former significantly differ from those of the latter. Indeed, for cells from young culture, the distribution map of the Young modulus presents features comparable to those detected in the cell stiffness map (Fig. 7a). This observed correlation is reflected by a linear dependence of k_{cell} on E (Fig. 8a, right) with a slope of 6.25 x 10^{-5} N m^{-1} kPa^{-1} (R^2 = 0.74). This linearity suggests that the cell wall elastic properties are intimately connected to the internal turgor pressure. For untreated cells of the mature culture, the range of E values enlarges towards lower and higher values, reflecting both the softening of the cell-wall upon ageing and the presence of the stiff fibrils. Oppositely, the range of k_{cell} values identified for mature cells reduces because cells harvested in the stationary phase are

in a physiological state which differs from that of cells in the mid-log phase, and the structural remodelling of the cell-wall may also impact on the k_{cell} values.[38]

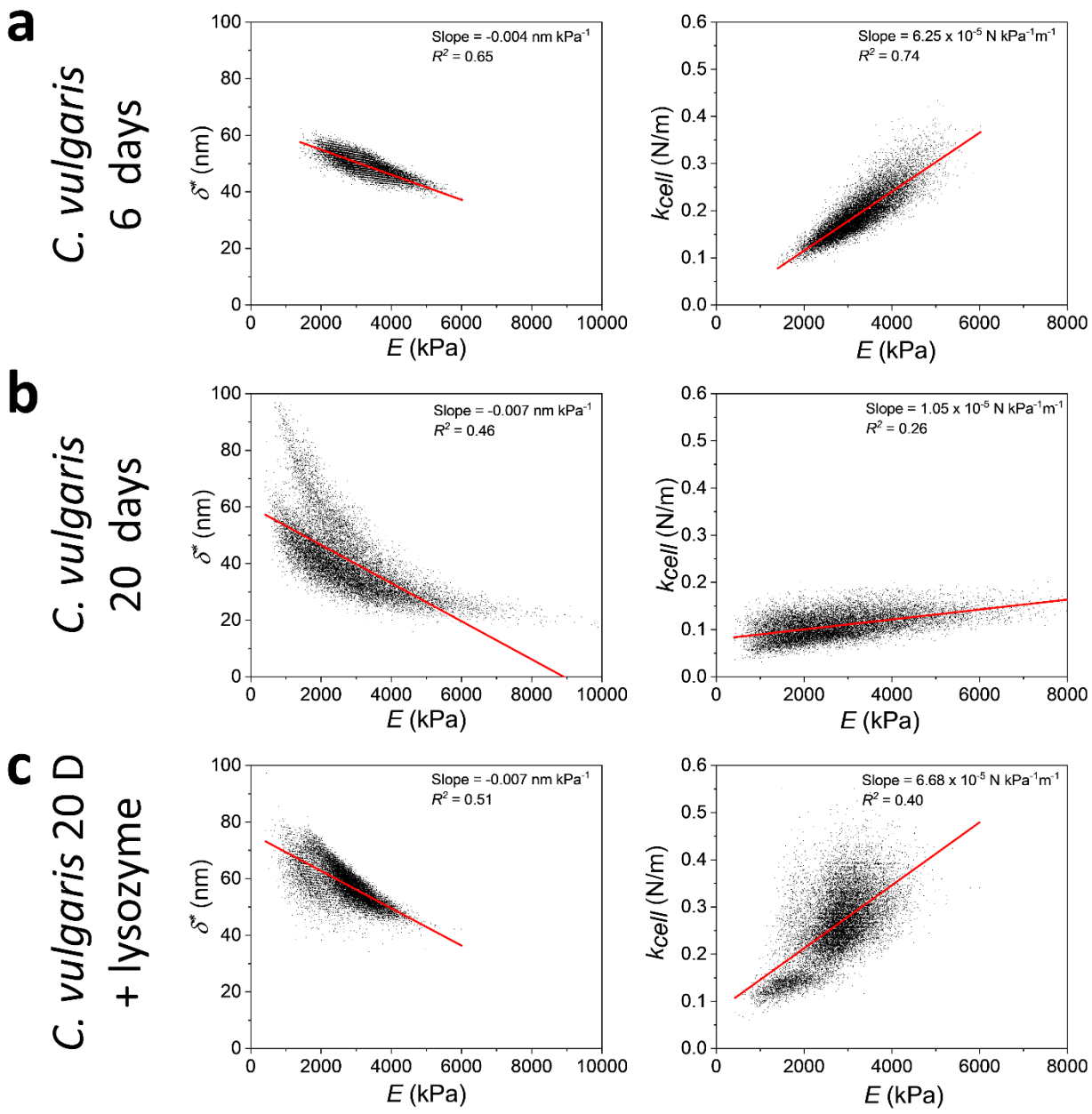

Figure 8. Dependence of the indentation δ^* and cell stiffness k_{cell} *on* Young modulus *E*. Plots of indentation δ^* *versus* Young modulus *E* (left column) and cell stiffness k_{cell} *versus* Young modulus *E* (right column) constructed from analysis of the 65536 force curves reported in the maps of Fig. 7 for cells from young (a), mature (b) and lysozyme-treated mature (c) cultures. Red lines correspond to the linear fit of the data in the scattered plots.

These two effects result in a lower slope of k_{cell} *vs.* E than that estimated from data collected on cells from the young culture, together with a loss of linearity as reflected in the corresponding R^2 value (Fig. 8b, right panel, slope = 1.05 x 10^{-5} N m^{-1} kPa^{-1}, R^2 = 0.26). Upon lysozyme treatment, spatial heterogeneities detected on the corresponding elasticity and cell stiffness maps (Fig. 7c) are not consistent with the above linearity evidenced for cells from the young culture (see Fig. 8a *versus* Fig. 8c). A linear regression of k_{cell} *versus* E data measured for lysozyme-treated cells provides indeed (Fig. 8c, right) a slope similar to that estimated for cells from the young culture (6.68 x 10^{-5} N m^{-1} kPa^{-1}) albeit with much poorer value of R^2 (= 0.40). Taken together, these result support the idea that lysozyme mediates both surface *and* intracellular changes.

To analyse the heterogeneity in the cell surface properties among a collection of multi-individual algal cells, we performed statistical analysis of the nanomechanical proxies E, k_{cell} and δ^* determined from analysis of several sets of 65536 force curves measured on 12 distinct cells from young culture, 13 cells from mature culture and 8 cells from the lysozyme-treated mature culture (1 set of 65536 force curves per cell). For each cell tested, results are compiled in the form of histograms representing the frequency distributions of the evaluated E, δ^* and k_{cell}. These histograms are subsequently fitted by means of one and two Gaussian distributions, and the R^2 values associated with these fits reflect the quality of the reconstruction of the histogram distribution (see the illustrative example given in Fig. 9a,b for the Young modulus). Box plots collecting the R^2 values corresponding to the adjustment of the distributions in E, δ^* and k_{cell} measured for all cells (either from young, mature or lysozyme-treated cultures) on the basis of a monomodal or a bimodal Gaussian distribution (denoted as ''1G'' and ''2G'' in Fig. 9, respectively) are presented in Fig. 9 c, d and e, respectively.

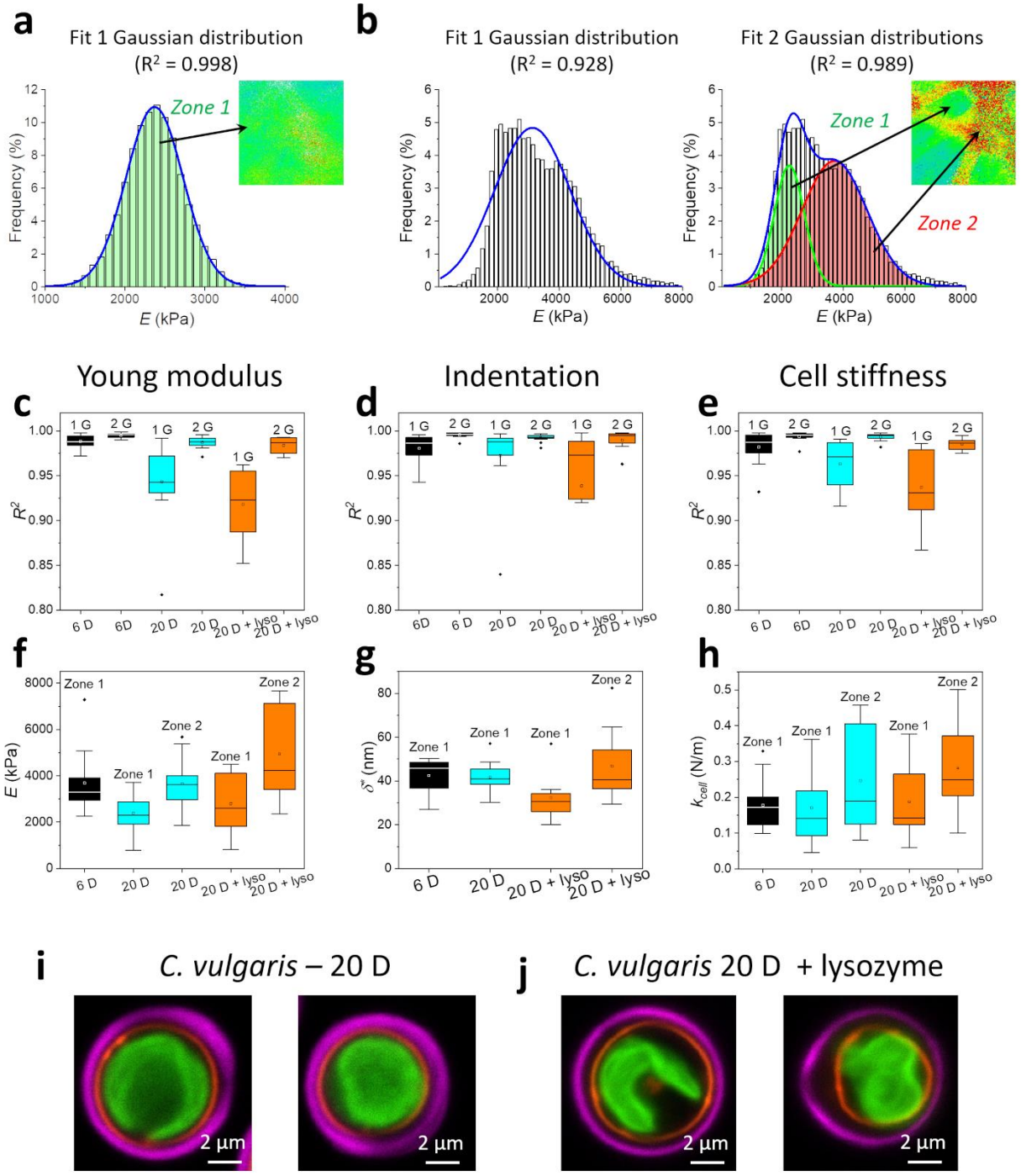

Figure 9. Statistical analysis of the evolution of the Young modulus *E*, indentation δ^* and cell stiffness k_{cell} upon ageing and lysozyme treatment. (a-b) Each frequency histogram of *E*, δ^* and k_{cell} generated from the 65536 force curves recorded on individual cells are fitted by mean of one (a, b left panel) or two (b, right panel) Gaussian distribution curves. The R^2 obtained for the two fits are presented in the box plots in (c-e) for each culture condition (*i.e.* young culture in black, mature culture in blue and lysozyme-treated mature culture in orange), for which the bottom and top of the box are the 25th and 75th percentiles, the line is the median and the dot is the mean. 1G and 2G stand for data fitting to one or two Gaussian distributions, respectively. When the mean value of R^2 corresponding to the fit of distribution to one Gaussian distribution is larger than 0.97,

histogram distribution is fitted by one Gaussian curve (a). When that mean R^2 value is lower than 0.97 (b, left panel), the maps are considered to be split into two distinct spatial areas with different defining nanomechanical properties (a, right panel, zone 1 and zone 2) and histograms are then fitted on the basis of two Gaussian distribution curves (b, right panel). The values of the maximun peak(s) of either one or two gaussian distribution curve(s) for E, δ^* and k_{cell} are compiled in the box plots in F, G and H, respectively. Data in (c-h) originate from measurements on 12 cells of young culture (black boxes), 13 cells from mature culture (blue boxes) and 8 cells from lysozyme-treated mature culture (orange boxes). (i-j) Confocal images of the cells AF (false-coloured in green), WGA-FITC (in pink) and FM4-64 (in red) stained structures on cells from mature (i) and lysozyme-treated mature (j) cultures.

When the mean R^2 value (represented in the box plot by a square symbol in the box) associated with the fitting of the histogram to a monomodal Gaussian distribution is larger than here-adopted value of 0.97, the mechanical data of the corresponding ensemble of cells (*i.e.* either the 12 cells from young culture, the 13 cells from mature culture or the 8 cells from the lysozyme-treated culture) are fitted by a single Gaussian distribution (Fig. 9a, and 9f, g and h). On the opposite, when mean R^2 value is lower than 0.97, we consider that the frequency distribution of E, δ^* and k_{cell} for each cell is associated with nanomechanical properties of two distinct cell surface regions (denoted hereafter as zone 1 and zone 2 at the surface of each individual cell), each region referring to the separate mode of a more appropriate (and thus adopted) bimodal Gaussian distribution (Fig. 9b, and 9f, g and h).

For cells from the young culture, the distributions in E, δ^* and k_{cell} values (Fig. 9c-h, black boxes) could all be satisfactorily adjusted with one Gaussian distribution model, which translates that analysed cells are relatively homogeneous in terms of surface feature (as connected to E) and of turgor pressure (as connected to k_{cell},[44]), in agreement with the maps displayed in Fig. 7 for the cells of the young culture and with the absence of any significantly structured layer from the topographical images given in Fig. 2. The surface heterogeneity among the 12 tested algal cells

harvested in the mid-log phase is also relatively weak, which is materialized by the narrow distribution of the E, δ^* and k_{cell} values encompassed within the 25-75% percentiles range of the box plots (corresponding to the height of the black boxes in Fig. 9f-h).

For cells from the non-treated mature culture, the presence of the fibrils at the cell surface imposes a fit of the distribution of the E values by a bimodal Gaussian distribution as the adjustment of data to a single distribution leads to a mean R^2 value of 0.94 (Fig. 9c, blue boxes). The unstructured matrix of algae cell-wall (which corresponds to the so-called zone 1 in Fig. 9f, blue box, cf. Fig. 9b) tends to soften upon ageing and some protruding fibrils (zone 2 in Fig. 9f, blue box, cf. Fig. 9b) tend to rigidify the cell surface, which supports the conclusions drawn from analysis of illustrative E map reported for selected individual cell in Fig. 7b. Unlike histogram of E values, δ^* histogram could be successfully fitted by means of a single Gaussian distribution (Fig. 9d, blue box) and the average value of δ^* overall analysed cells from the mature culture did not significantly differ from that of cells from young culture (Fig. 9g, black box). The entanglement of overlapping fibrils at the surface makes more complex the interpretation of the relationship between the surface Young modulus and the indentation depth, as invoked earlier from the loss of linearity between E vs. δ^* for individual cell from mature culture (Fig. 8b). The presence of the fibrils also impacts notably on the k_{cell} distribution, as high levels of intra- and inter-cellular heterogeneities in k_{cell} values (as reflected by the data dispersion in the box plot and by the occurrence of two spatially distinct k_{cell}-zones) are derived in zone 1 *and* zone 2 for cells from the mature culture, which strikingly contrasts with the situation depicted for cells from the young culture (Fig. 9e, h, blue boxes).

The main conclusion from the statistical analysis of the cells harvested from the lysozyme-treated exponential phase culture is that the enzymatic treatment enhances both aforementioned intra-and inter-cellular heterogeneities, which is manifested by poor values of R^2 when fitting histograms of E, δ^* and k_{cell} values to a single Gaussian distribution (Fig. 9c-e, orange boxes). Although the surface morphology of the cells from the lysozyme-treated culture looks like that of the cells from the young culture, their mechanical properties differ significantly. Lysozyme is known to remove the *N*-acetyl-D-glucosamine protective layer at the algal surface.[5] Similarly, other enzymes, such as chitinase, are able to degrade the *Chlorella* chitin layer.[6] However, no significant loss of mechanical stability has been reported after treating microbial cell with lysozyme or chitinase alone.[5, 45] Here, interestingly, although AFM imaging suggests that lysozyme treatment strips the rigid fibrils, the distributions in E values according to two distinct spatial zones indicate that fibrils still contribute to cell surface nanomechanics (Fig. 9f, orange boxes). Gerken *et al*. reported that lysozyme action leads to a significant increase in the cell wall thickness.[5] This is in qualitative agreement with our confocal images which confirm that, although lysozyme treatment slims down the *N*-acteyl-D-glucosamine layer, the total cell-wall thickness is not affected or increases in some specific spots (Fig 9i, j). This could explain why the critical indentation δ^* reaches highest values for cells from the lysozyme-treated culture (Fig. 9 g) despite of the partial removal of the peripheral fibril layer upon enzyme action. Not surprisingly, values of k_{cell} are highly scattered for enzyme-treated cells, which is intuitively expected for an algal treatment that affects both the intracellular and the surface components of a population of cells in the stationary phase that natively display heterogeneous k_{cell}-features. Altogether, our results reveal some intimate connections between enzyme-mediated effects on intracellular and cell envelop properties, and they underline the added value brought by the combination of techniques able to probe bio-surfaces at the relevant nanoscale

and/or microscale (AFM and confocal microscopy) to decipher the complex action of enzyme treatments as that of lysozyme in view of optimizing industrial bioprocesses (*e.g.* lipid extraction).

4. CONCLUSIONS

In summary, we exploit the different modalities offered by AFM in association with confocal microscopy to gain a better understanding of the cell wall properties of *C. vulgaris* grown under different conditions. We found that the algal surface morphology switches from an unstructured layer to a fibrillated network as the culture gets older, and this organisation vanishes upon lysozyme treatment. Chemical identification of the fibrils was achieved at various scales by using WGA-lectin to both stain the chitin-like layer at the surface of cells from mature culture and functionalize AFM tip to probe molecular cell-to-lectin adhesion events over the cell surface. Correlations were further established between lysozyme-mediated effects on cell properties as identified by confocal imaging after staining of intracellular organelles and by spatially-resolved nanomechanical properties of cell envelops deciphered by nanoindentation atomic force spectroscopy. This original combination of tools evidenced the dual action of the enzyme*, i.e.* degradation of the fibrillated structure at the cell surface and increase in the size of intracellular lipid droplets. In addition to providing fundamental insights into *C. vulgaris* physico-chemical properties, the here-developed methodology and reported results may be of interest for industries having the objective to develop technologies that facilitate lipids and proteins extraction from microalgae.

CONFLICTS OF INTEREST

The authors declare no conflict of interest.

ACKNOWLEDGMENTS

This work was supported by ANR grant ANR-20-CE34-0005-01 to AB. AB and BS acknowledge the Pôle scientifique OTELO for the support of the Interdisciplinary grant FLUOCHLOR. This work was partly carried out in the Pôle de compétences Physico-Chimie de l'Environnement, LIEC laboratory UMR 7360 CNRS – Université de Lorraine.

AUTHORS CONTRIBUTIONS

Jérôme F. L. Duval: Conceptualization, methodology, software, validation, formal analysis, investigation, writing, supervision, project administration.
Angelina Razafitianamaharavo: Conceptualization, methodology, software, validation, formal analysis, investigation, visualization.
Isabelle Bihannic: Conceptualization, methodology, validation, formal analysis, investigation.
Marc Offroy: Conceptualization, methodology, software, validation, formal analysis.
Nicolas Lesniewska : Methodology, validation, resources, formal analysis, investigation.
Bénédicte Sohm : Conceptualization, methodology, resources, funding acquisition.
Hélène Le Cordier : Methodology, resources.
Christian Mustin : Conceptualization, methodology.
Christophe Pagnout: Conceptualization, methodology, resources.
Audrey Beaussart : Conceptualization, methodology, validation, formal analysis, investigation, writing, visualisation, supervision, project administration, funding acquisition.

REFERENCES

1. Y. H. Kim, Y. K. Choi, J. Park, S. Lee, Y. H. Yang, H. J. Kim, T. J. Park, Y. H. Kim, S. H. Lee, Ionic liquid-mediated extraction of lipids from algal biomass. Bioresource Technology (2012), 312-315.
2. T. R. Zinkone, I. Gifuni, L. Lavenant, J. Pruvost, L. Marchal, Bead milling disruption kinetics of microalgae: Process modeling, optimization and application to biomolecules recovery from Chlorella sorokiniana. Bioresource Technology (2018), 458-465.
3. B. H. J. Yap, G. J. Dumsday, P. J. Scales, G. J. O. Martin, Energy evaluation of algal cell disruption by high pressure homogenisation. Bioresource Technology (2015), 280-285.
4. V. Skorupskaite, V. Makareviciene, E. Sendzikiene, M. Gumbyte, Microalgae Chlorella sp. cell disruption efficiency utilising ultrasonication and ultrahomogenisation methods. Journal of Applied Phycology 4 (2019), 2349-2354.
5. H. G. Gerken, B. Donohoe, E. P. Knoshaug, Enzymatic cell wall degradation of Chlorella vulgaris and other microalgae for biofuels production. Planta 1 (2013), 239-253.
6. G. Canelli, P. M. Martinez, B. M. Hauser, I. Kuster, Z. Rohfritsch, F. Dionisi, C. J. Bolten, L. Neutsch, A. Mathys, Tailored enzymatic treatment of Chlorella vulgaris cell wall leads to effective disruption while preserving oxidative stability. Lwt-Food Science and Technology (2021).
7. R. Soto-Ramirez, M. G. Lobos, O. Cordova, P. Poirrier, R. Chamy, Effect of growth conditions on cell wall composition and cadmium adsorption in Chlorella vulgaris: A new approach to biosorption research. Journal of Hazardous Materials (2021).
8. S. Hena, L. Gutierrez, J. P. Croue, Removal of pharmaceutical and personal care products (PPCPs) from wastewater using microalgae: A review. Journal of Hazardous Materials (2021).
9. A. Rahman, S. L. Pan, C. Houston, T. Selvaratnam, Evaluation of Galdieria sulphuraria and Chlorella vulgaris for the Bioremediation of Produced Water. Water 9 (2021).
10. S. N. Tolboom, D. Carrillo-Nieves, M. D. Rostro-Alanis, R. D. Quiroz, D. Barcelo, H. M. N. Iqbal, R. Parra-Saldivar, Algal-based removal strategies for hazardous contaminants from the environment - A review. Science of the Total Environment (2019), 358-366.
11. L. Xia, R. Huang, Y. T. Li, S. X. Song, The effect of growth phase on the surface properties of three oleaginous microalgae (Botryococcus sp FACGB-762, Chlorella sp XJ-445 and Desmodesmus bijugatus XJ-231). Plos One 10 (2017).
12. F. Pillet, E. Dague, J. P. Ilic, I. Ruzic, M. P. Rols, N. I. Denardis, Changes in nanomechanical properties and adhesion dynamics of algal for cells during their growth updates. Bioelectrochemistry (2019), 154-162.
13. X. Z. Zhang, P. Amendola, J. C. Hewson, M. Sommerfeld, Q. Hu, Influence of growth phase on harvesting of Chlorella zofingiensis by dissolved air flotation. Bioresource Technology (2012), 477-484.
14. S. J. Lee, S. B. Kim, J. E. Kim, G. S. Kwon, B. D. Yoon, H. M. Oh, Effects of harvesting method and growth stage on the flocculation of the green alga Botryococcus braunii. Letters in Applied Microbiology 1 (1998), 14-18.
15. M. K. Danquah, B. Gladman, N. Moheimani, G. M. Forde, Microalgal growth characteristics and subsequent influence on dewatering efficiency. Chemical Engineering Journal 1-3 (2009), 73-78.
16. H. J. Butt, M. Jaschke, Calculation of thermal noise in atomic force microscopy. Nanotechnology 1 (1995), 1-7.

17. E. Kapaun, W. Reisser, A CHITIN-LIKE GLYCAN IN THE CELL-WALL OF A CHLORELLA SP (CHLOROCOCCALES, CHLOROPHYCEAE). Planta 4 (1995), 577-582.
18. S. Weber, P. M. Grande, L. M. Blank, H. Klose, Insights into cell wall disintegration of Chlorella vulgaris. Plos One 1 (2022).
19. Alma Carolina Gálvez-Iriqui, Maribel Plascencia-Jatomea, Silvia Bautista-Baños, Lysozymes: characteristics, mechanism of action and technological applications on the control of pathogenic microorganisms. Revista Mexicana de Fitopatología 3 (2020), 360-360-383.
20. T. Wu, Q. Jiang, D. Wu, Y. Hu, S. Chen, T. Ding, X. Ye, D. Liu, J. Chen, What is new in lysozyme research and its application in food industry? A review. Food Chem (2019), 698-709.
21. A. Beaussart, C. Pechoux, P. Trieu-Cuot, P. Hols, M. Y. Mistou, Y. F. Dufrene, Molecular mapping of the cell wall polysaccharides of the human pathogen Streptococcus agalactiae. Nanoscale 24 (2014), 14820-14827.
22. S. El-Kirat-Chatel, A. Beaussart, D. Alsteens, A. Sarazin, T. Jouault, Y. F. Dufrene, Single-molecule analysis of the major glycopolymers of pathogenic and non-pathogenic yeast cells. Nanoscale 11 (2013), 4855-4863.
23. A. Lakshminarayanan, M. Richard, B. G. Davis, Studying glycobiology at the single-molecule level. Nature Reviews Chemistry 8 (2018), 148-159.
24. M. Rief, M. Gautel, F. Oesterhelt, J. M. Fernandez, H. E. Gaub, Reversible unfolding of individual titin immunoglobulin domains by AFM. Science 5315 (1997), 1109-1112.
25. R. Loris, T. Hamelryck, J. Bouckaert, L. Wyns, Legume lectin structure. Biochimica Et Biophysica Acta-Protein Structure and Molecular Enzymology 1 (1998), 9-36.
26. M. Yamamoto, I. Kurihara, S. Kawano, Late type of daughter cell wall synthesis in one of the Chlorellaceae, Parachlorella kessleri (Chlorophyta, Trebouxiophyceae). Planta 6 (2005), 766-775.
27. X. Han, Y. S. Wong, N. F. Y. Tam, Surface complexation mechanism and modeling in Cr(III) biosorption by a microalgal isolate, Chlorella miniata. Journal of Colloid and Interface Science 2 (2006), 365-371.
28. Hiroshi Takeda, Chemical composition of cell walls as a taxonomical marker. Journal of Plant Research 3 (1993), 195-200.
29. Hp Kusumaningrum, M Zainuri, Improvement of Nutrition Production by Protoplast Fusion Techniques in *Chlorella vulgaris*. Journal of food processing and technology 1 (2018).
30. K. During, P. Porsch, A. Mahn, O. Brinkmann, W. Gieffers, The non-enzymatic microbicidal activity of lysozymes. Febs Letters 2-3 (1999), 93-100.
31. B. Masschalck, C. W. Michiels, Antimicrobial properties of lysozyme in relation to foodborne vegetative bacteria. Critical Reviews in Microbiology 3 (2003), 191-214.
32. A. Pellegrini, U. Thomas, P. Wild, E. Schraner, R. Von Fellenberg, Effect of lysozyme or modified lysozyme fragments on DNA and RNA synthesis and membrane permeability of Escherichia coli. Microbiological Research 2 (2000), 69-77.
33. H. S. Cho, Y. K. Oh, S. C. Park, J. W. Lee, J. Y. Park, Effects of enzymatic hydrolysis on lipid extraction from Chlorella vulgaris. Renewable Energy (2013), 156-160.
34. D. Coelho, P. A. Lopes, V. Cardoso, P. Ponte, J. Bras, M. S. Madeira, C. M. Alfaia, N. M. Bandarra, H. G. Gerken, Cmga Fontes, J. A. M. Prates, Novel combination of feed enzymes to improve the degradation of Chlorella vulgaris recalcitrant cell wall. Scientific Reports (2019).
35. A. Jaussaud, J. Lupette, J. Salvaing, J. Jouhet, O. Bastien, M. Gromova, E. Marechal, Stepwise Biogenesis of Subpopulations of Lipid Droplets in Nitrogen Starved Phaeodactylum tricornutum Cells. Frontiers in Plant Science (2020).

36. J. Jung, S. J. Hong, H. B. Kim, G. Kim, M. Lee, S. Shin, S. Lee, D. J. Kim, C. G. Lee, Y. Park, Label-free non-invasive quantitative measurement of lipid contents in individual microalgal cells using refractive index tomography. Scientific Reports (2018).
37. M. F. De Souza, M. A. Rodrigues, S. P. Freitas, E. P. D. Bon, Effect of milling and enzymatic hydrolysis in the production of glucose from starch-rich Chlorella sorokiniana biomass. Algal Research-Biomass Biofuels and Bioproducts (2020).
38. G. Francius, P. Polyakov, J. Merlin, Y. Abe, J. M. Ghigo, C. Merlin, C. Beloin, J. F. L. Duval, Bacterial Surface Appendages Strongly Impact Nanomechanical and Electrokinetic Properties of Escherichia coli Cells Subjected to Osmotic Stress. Plos One 5 (2011).
39. M. Offroy, A. Razafitianamaharavo, A. Beaussart, C. Pagnout, J. F. L. Duval, Fast automated processing of AFM PeakForce curves to evaluate spatially resolved Young modulus and stiffness of turgescent cells. Rsc Advances 33 (2020), 19258-19275.
40. C. Pagnout, A. Razafitianamaharavo, B. Sohm, C. Caillet, A. Beaussart, E. Delatour, I. Bihannic, M. Offroy, J. F. L. Duval, Osmotic stress and vesiculation as key mechanisms controlling bacterial sensitivity and resistance to TiO2 nanoparticles. Communications Biology 1 (2021).
41. N. Gavara, R. S. Chadwick, Determination of the elastic moduli of thin samples and adherent cells using conical atomic force microscope tips. Nature Nanotechnology 11 (2012), 733-736.
42. Ian N. Sneddon, The relation between load and penetration in the axisymmetric boussinesq problem for a punch of arbitrary profile. International Journal of Engineering Science 1 (1965), 47-57.
43. G. Canelli, P. M. Martinez, S. Austin, M. E. Ambuhl, F. Dionisi, C. J. Bolten, R. Carpine, L. Neutsch, A. Mathys, Biochemical and Morphological Characterization of Heterotrophic Crypthecodinium cohnii and Chlorella vulgaris Cell Walls. Journal of Agricultural and Food Chemistry 7 (2021), 2226-2235.
44. M. Arnoldi, M. Fritz, E. Bauerlein, M. Radmacher, E. Sackmann, A. Boulbitch, Bacterial turgor pressure can be measured by atomic force microscopy. Phys. Rev. E 1 (2000), 1034-1044.
45. J. J. Thwaites, U. C. Surana, A. M. Jones, Mechanical properties of *Bacillus subtilis* cell-walls - Effects of ions and lysozyme. Journal of Bacteriology 1 (1991), 204-210.